

Impacts of Climate Modes on Air–Sea Heat Exchange in the Red Sea

YASSER ABUALNAJA,* VASSILIS P. PAPADOPOULOS,⁺ SIMON A. JOSEY,[#]
IBRAHIM HOTEIT,[@] HARILAOS KONTOYIANNIS,⁺ AND DIONYSIOS E. RAITOS[&]

* *Red Sea Research Centre, King Abdullah University of Science and Technology, Thuwal, Saudi Arabia*

⁺ *Hellenic Centre for Marine Research, Anavissos, Greece*

[#] *National Oceanography Centre, Southampton, United Kingdom*

[@] *Physical Science and Engineering Division, King Abdullah University of Science and
Technology, Thuwal, Saudi Arabia*

[&] *Plymouth Marine Laboratory, Plymouth, Devon, United Kingdom*

(Manuscript received 29 May 2014, in final form 12 November 2014)

ABSTRACT

The impacts of various climate modes on the Red Sea surface heat exchange are investigated using the MERRA reanalysis and the OAF flux satellite reanalysis datasets. Seasonality in the atmospheric forcing is also explored. Mode impacts peak during boreal winter [December–February (DJF)] with average anomalies of 12–18 W m⁻² to be found in the northern Red Sea. The North Atlantic Oscillation (NAO), the east Atlantic–west Russia (EAWR) pattern, and the Indian monsoon index (IMI) exhibit the strongest influence on the air–sea heat exchange during the winter. In this season, the largest negative anomalies of about –30 W m⁻² are associated with the EAWR pattern over the central part of the Red Sea. In other seasons, mode-related anomalies are considerably lower, especially during spring when the mode impacts are negligible. The mode impacts are strongest over the northern half of the Red Sea during winter and autumn. In summer, the southern half of the basin is strongly influenced by the multivariate ENSO index (MEI). The winter mode-related anomalies are determined mostly by the latent heat flux component, while in summer the shortwave flux is also important. The influence of the modes on the Red Sea is found to be generally weaker than on the neighboring Mediterranean basin.

1. Introduction

The Red Sea is a marginal, elongated basin lying between northeastern Africa and the Arabian Peninsula. It contains one of the most valuable marine ecosystems of the global ocean that features an extensive chain of nearshore coral reefs. Almost entirely surrounded by arid and semiarid areas, the Red Sea receives an extremely small amount of precipitation and negligible freshwater from river runoff. At the same time, the evaporation rate is one of the world's highest exceeding 2 m yr⁻¹, and it is considered one of the warmest seas in the world (Morcos 1970; Ahmad and Sultan 1989; Sofianos and Johns 2002; Belkin 2009; Raitos et al. 2011). The consequent water deficit is counterbalanced by an inverse estuarine flow

through the narrow (25 km wide) Bab el Mandeb Strait at the southernmost edge of the basin (Murray and Johns 1997; Sofianos and Johns 2002; Yao et al. 2014a,b). These characteristics result in surface salinity values that over the northern part exceed 40, making this part of the basin one of the most saline in the World Ocean. Despite these unique features, oceanographic studies in the Red Sea are limited and based on scarce field works and mostly on numerical simulations. This is particularly true for the air–sea heat fluxes regime.

Surface heat exchange fuels ocean and atmosphere dynamics and affects several important properties like the surface water buoyancy and the air stability of the atmospheric boundary layer. In oceanographic terms, the air–sea heat exchange directly influences the sea surface temperature and indirectly, through latent heat (evaporation), the surface salinity. Thus, the surface heat exchange is a crucial factor for the thermohaline circulation of the Red Sea basin. Atmospheric parameters like air temperature, specific humidity, cloudiness,

Corresponding author address: Yasser Abualnaja, Red Sea Research Centre, King Abdullah University of Science and Technology, Thuwal 23955-6900, Saudi Arabia.
E-mail: yasser.abualnaja@kaust.edu.sa

and wind speed and direction, regulate the air–sea heat fluxes and vice versa. These atmospheric variables are intimately linked to the general atmospheric circulation described by the sea level pressure (SLP) field. The influence of the large-scale atmospheric circulation on the air–sea heat flux, in a range of ocean basins, on various temporal and spatial scales has been considered in various studies (e.g., Cayan 1992; Alexander and Scott 1997; Josey 2003; Bond and Cronin 2008; Josey et al. 2011; Papadopoulos et al. 2012a,b,c).

Recently, Papadopoulos et al. (2013, hereinafter P13) identified particular synoptic SLP fields favoring winter extremes of the turbulent components of the air–sea heat fluxes over the northern part of the Red Sea. The study at hand extends the analysis of P13, focusing on the impact of climate modes on the surface net heat exchange over the entire basin covering the four seasons of the year. The effects of climatic indices are analyzed according to the method introduced by Josey et al. (2011, hereinafter JST11). Moreover, the analysis performed in the Mediterranean Sea by JST11 provides a reference for comparison between the two neighboring basins. A total of nine climatic indices of potential relevance to the Red Sea climate regime have been chosen here. In addition to the four indices chosen by JST11, we include five more, taking into account the location of the Red Sea, which lies in a transitional region with potential influence from the Atlantic, Indian, and Pacific Oceans. The manuscript is organized as follows: The datasets are presented in section 2, while the methodology is explained in section 3. Section 4 presents the seasonal climatology of the heat flux and the wind regime, and section 5 describes the impacts of the climate modes employed in the study. The results of our analysis are discussed in section 6, and finally section 7 summarizes the main findings of the study.

2. Datasets

To examine the air–sea heat fluxes over the Red Sea, we employ monthly-mean values from two datasets. The first is the NASA Modern-Era Retrospective Analysis for Research and Applications (MERRA; Rienecker et al. 2011). The MERRA assimilation spans the period 1979–present and features a finer resolution of $2/3^\circ \times 1/2^\circ$ than earlier products. The heat flux values used in our study span the 35 yr from 1979 to 2013. The second dataset is the objectively analyzed air–sea fluxes (OAFlux; Yu et al. 2008) dataset produced at the Woods Hole Oceanographic Institution. In this dataset, surface net heat flux is derived by the combination of two products with each one of them having a different origin. The radiative terms, shortwave and longwave radiation, come from ISCCP flux data (FD)

project and are determined using a radiative transfer model from the Goddard Institute for Space Studies (Zhang et al. 2004). The turbulent terms, latent and sensible heat, come from OAFlux (Yu et al. 2008). OAFlux data have 1° resolution and span the period 1983–2009. Maps showing the Red Sea location and the grid points of these two datasets are presented in Fig. 1.

To determine the influence of surface meteorological variables (mean SLP, dewpoint temperature, and wind speed) and sea surface temperature on the surface fluxes, we employ the ERA-Interim (Dee et al. 2011) reanalysis dataset for the period 1979–2013. Note we also employ MERRA SLP and wind fields to check that our climate index-based regressions are not sensitive to the choice of reanalysis (see section 5). Climatic indices of atmospheric and oceanic origin that might have a potential influence on the Red Sea climate are employed to investigate their impact on the air–sea heat exchange. Namely, these are the North Atlantic Oscillation (NAO), the east Atlantic pattern (EA), the west Pacific pattern (WP), the east Atlantic–west Russia pattern (EAWR), the Scandinavian pattern (SCA), the Polar–Eurasia pattern (POL), the multivariate El Niño–Southern Oscillation index (MEI), the Indian Ocean dipole index (IOD), and a version of the Indian monsoon index (IMI). Relevant time series for NAO, EA, WP, EAWR, SCA, POL, and MEI are obtained from the NOAA/Climate Prediction Center (CPC). With the exception of MEI, these indices represent modes of Northern Hemisphere SLP variability produced using rotated EOF analysis (Barnston and Livezey 1987). This separation of variance by indices is a mathematical decomposition of temporally evolving complex hemispheric SLP patterns that has been shown to be a useful approach in many studies across a range of fields (e.g., Josey and Marsh 2005; JST11; Lim 2014; Martínez-Asensio et al. 2014). The MEI is a multivariate index introduced in an attempt to best represent the ENSO phenomenon (Wolter and Timlin 2011). Monthly time series of IOD are produced according to Saji et al. (1999) using sea surface temperature (SST) from the OAFlux archive. A version of the IMI is employed and defined using ERA-Interim fields as the averaged zonal wind shear between 850 and 200 hPa (U850–U200) geopotential heights over the area defined by 5° – 20° N and 40° – 80° E (Wang and Fan 1999). Both IOD and IMI are normalized by dividing by their standard deviations.

3. Method

The main scope of the present study is to identify the influence of atmospheric forcing associated with several climatic indices on the surface net heat flux over the Red Sea. Prior to that, the seasonal-mean

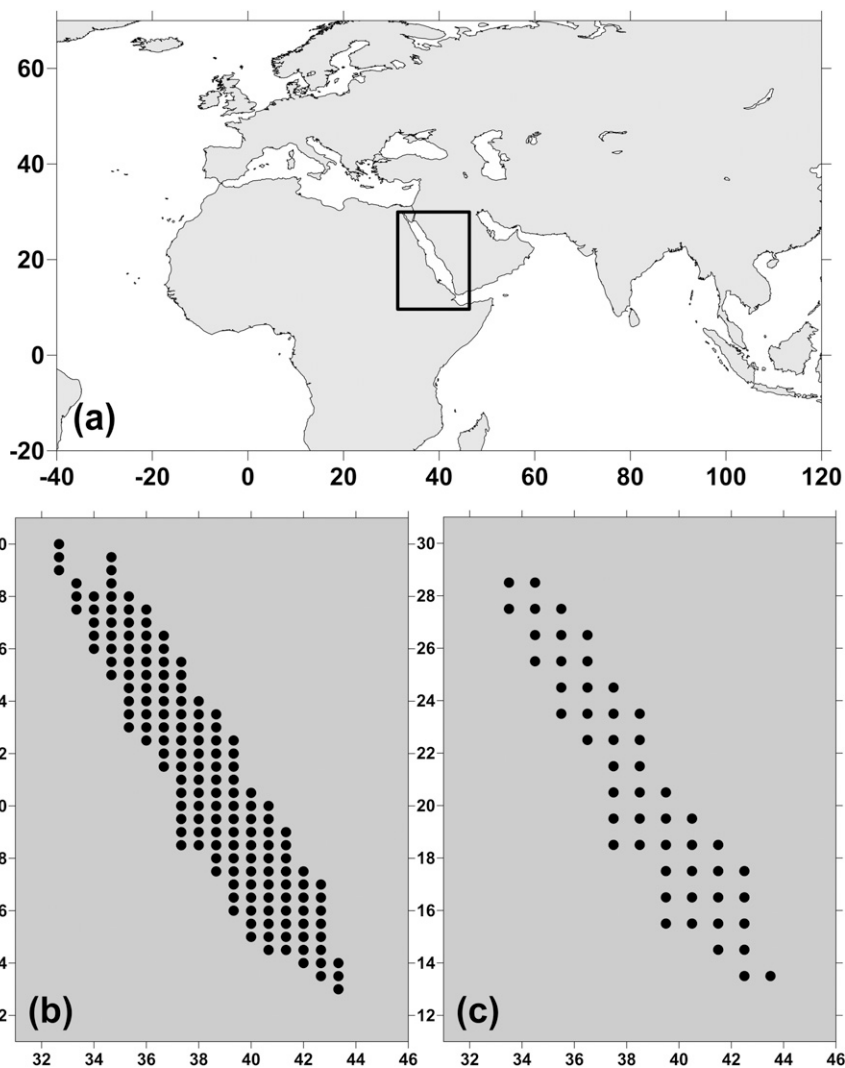


FIG. 1. The (a) Red Sea region and the (b) MERRA and (c) OAF flux grid points.

climatologies (35-yr mean values for each grid point) for winter [December–February (DJF)], spring [March–May (MAM)], summer [June–August (JJA)], and autumn [September–November (SON)] are presented using the MERRA dataset. The mode impacts on surface net heat flux are quantified according to the method introduced by JST11. Thus, we calculate the heat flux anomaly that corresponds to a unit positive value of each index (anomaly normalization). To calculate this heat flux anomaly, months with index absolute values greater than 1 are segregated out separately for each season. Heat flux anomalies at each grid point for the sequestered months are then divided by the corresponding index value; hence, the positive unit index anomaly is produced (normalized anomaly). Finally, the composite anomaly at each grid point is calculated by averaging the anomalies corresponding to each season. To fully explore the index-related

atmospheric forcing that gives rise to heat flux anomalies, we also examine the impact of a positive unit index on each of the net heat flux components. The oceanographic convention for the heat flux is adopted according to which positive heat flux corresponds to heat gain by the sea and vice versa. Furthermore, the contribution of atmospheric factors like the specific humidity and the wind field to the air–sea heat exchange variations over the Red Sea is also investigated. To identify the seasonal variability, we use the same scale for maps referring to different seasons of the year where necessary.

4. Heat flux and wind climatology

Figure 2 shows the climatology of the net heat exchange for the four typical seasons of the Northern Hemisphere. Winter (DJF), spring (MAM), summer (JJA), and autumn

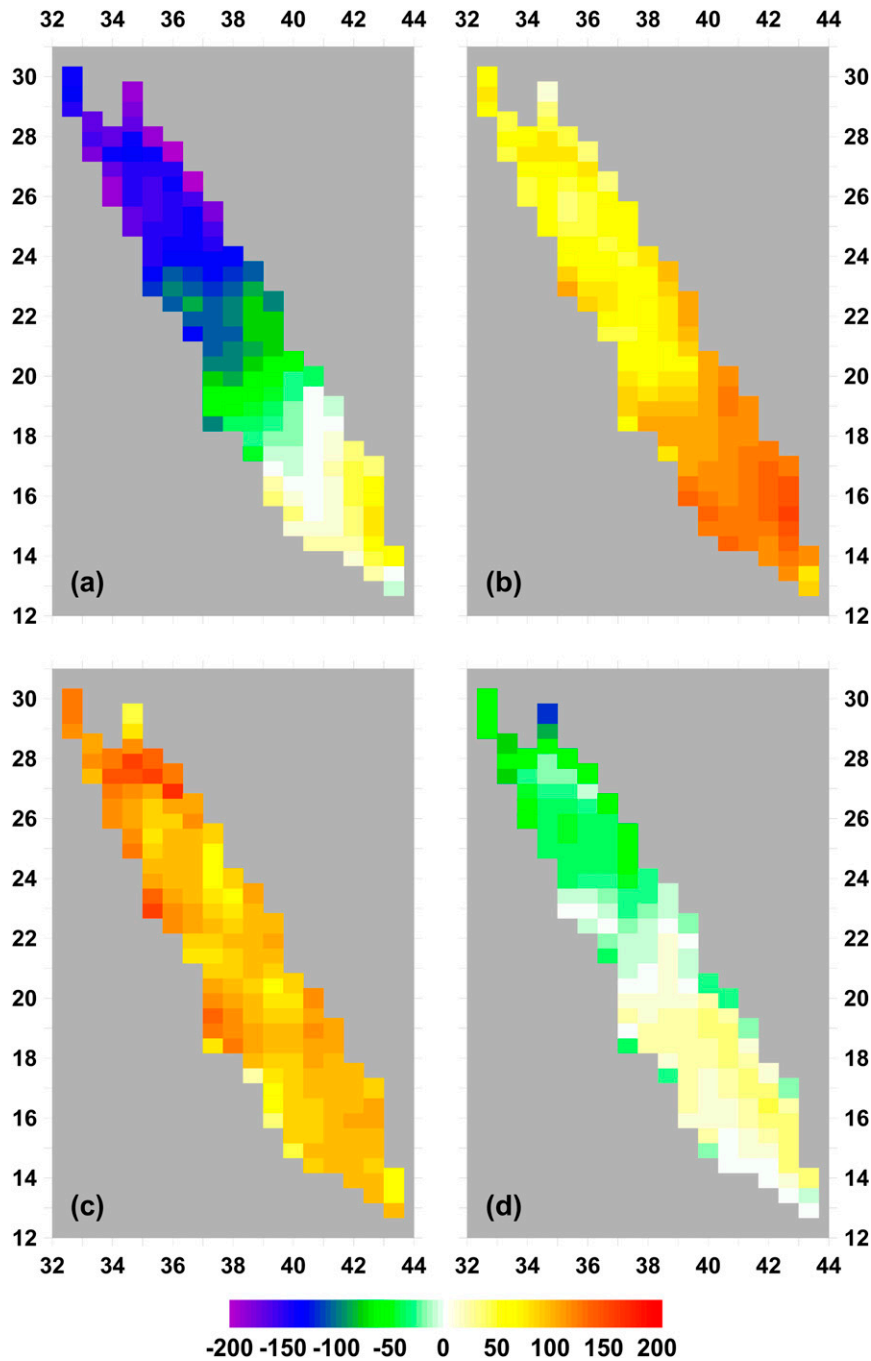


FIG. 2. Net heat flux (W m^{-2}) climatology based on 1979–2013 MERRA archive for (a) winter, (b) spring, (c) summer, and (d) autumn.

(SON) seasonal-mean values presented here are based on the MERRA dataset. The winter net heat flux (Q_{net}) values show a clear meridional gradient (Fig. 2a). Mean values reaching -200 W m^{-2} are observed over the northern part of the basin, especially close to the Saudi coastline, while heat gain by the sea up to $60\text{--}80 \text{ W m}^{-2}$ is observed over the southernmost Red Sea. During spring

(Fig. 2b), heat gain is observed over the whole basin, weak over the north, and much higher over the south with maximum values exceeding 150 W m^{-2} . Summer is also characterized by a positive net heat flux over the entire Red Sea 160 W m^{-2} are found in the northern half of the basin, while the lowest heat gain is found over the southern half

with values less than 30 W m^{-2} along the African coastline. Autumn can be considered an almost “neutral” season for the whole basin with low heat loss over the north and gain over the south (Fig. 2d). In terms of spatial distribution, autumn is somewhat similar to the winter pattern as both show a meridional gradient with heat loss in the north and gain in the south. This gradient is also obvious, yet without sign reversion between the north and south during spring, but a reverse meridional gradient occurs during summer when it is the northern basin that experiences the stronger heat gain. Analysis of individual heat flux components (not shown) indicates that this is because of reduced shortwave radiation values over the southern part of the basin.

One of the most important atmospheric variables with a high contribution to the heat flux regime is the wind that has the potential to be important in all seasons. Wind speed and direction have a strong influence on the other variables that determine the sea surface heat exchange through advection of different air masses. Air temperature, specific humidity, cloudiness, and even the sea surface temperature (in terms of upwelling or driving the surface circulation) are all directly or indirectly associated with the prevailing wind field. Thus, in addition to the net heat flux, we have investigated the wind climatology over the Red Sea. Figure 3 shows the seasonal wind field as derived from ERA-Interim for 1979–2013. During winter, northwest winds prevail over the northern part, whereas southeast winds blow over the southern part (Fig. 3a). The southeast winds over the southernmost part of the basin weaken during spring (Fig. 3b) and vanish during summer (Fig. 3c) when a uniform field of northwest winds prevails over the whole basin, yet stronger over the north. In autumn (Fig. 3d), the southeast winds begin to appear again, following the general winter monsoonal regime of the Arabian Sea that is the factor affecting the wind regime of the southern basin (Clifford et al. 1997; Sofianos and Johns 2003). With the exception of summer, a significant area of the basin extending between 16° and 20°N experiences very weak winds. In general, stronger winds blow over the northern part of the Red Sea for most of the year. This fact plays a significant role in establishing the north–south gradient in the heat exchange since stronger wind is associated with enhanced heat loss from the sea surface through latent heat.

5. Climatic index characteristics

We will show later (section 6b) that of the nine indices considered, six (the NAO, EA, EAWR, MEI, IOD, and IMI) have a considerable impact on the air–sea heat flux over the Red Sea. For a better understanding of

the effects of these modes, we present the SLP and wind anomaly corresponding to a unit positive index of the most influential indices for winter (DJF) and summer (JJA) months for the 35 yr from 1979 to 2013. Figure 4 presents the winter characteristics of the climate modes over a broad area surrounding the Red Sea. The eastern flank of the NAO-related meridional SLP anomaly dipole in the Atlantic Ocean between the Azores and Iceland can be recognized. The EA is characterized by a domain of negative anomaly north of 50°N and a weaker positive one over the central Mediterranean Sea and northern Africa. The EAWR pattern exhibits two centers of opposite phases between Europe and western Russia. The EA, MEI, and IOD are found to have minor impacts on SLP over our specified area. The IMI shows a positive pole over central Europe, the Mediterranean Sea, and North Africa. We have repeated the mode-based anomaly analysis using MERRA SLP and wind fields for the calculations. This enables us to directly compare the climate index regressions obtained from ERA-Interim (Fig. 4) with those from MERRA (Fig. 5). Comparison of the two figures clearly shows that the climate index regressions are largely the same for both ERA-Interim and MERRA, so the choice between these reanalyses does not significantly affect our results. Note further that the mode signatures in SLP weaken considerably during summer (Fig. 6).

It is noteworthy that most of the indices show a minor impact on the wind field over the Red and Arabian Seas during both seasons. This fact indicates a possibly minor effect of the modes on the wind over the two sea areas and a rather stable seasonal wind regime. A determinant factor favoring a stable wind regime, mostly affecting the wind direction, is the morphology of the Red Sea. Extended mountain chains along the African and Arabian Peninsula coastlines channel the airstream to follow the along-axis direction (Patzert 1974). The major question here is if and how much each of the above patterns affects the Red Sea atmospheric forcing and consequently the air–sea heat fluxes.

In their study, JST11 used the four modes of atmospheric variability from the NOAA/CPC analysis that have a strong expression in the North Atlantic/European region. In our study, given the wider domain, we also explore the impact of the NOAA/CPC WP and POL patterns. By definition, all these modes can act independently as orthogonal modes derived by EOF analysis (Barnston and Livezey 1987; Rogers 1990). In addition, given the geographic location of the Red Sea and its influence by the Indian Ocean monsoons, we explore the potential impacts of the Indo-Pacific MEI, IOD, and IMI climatic mode indices.

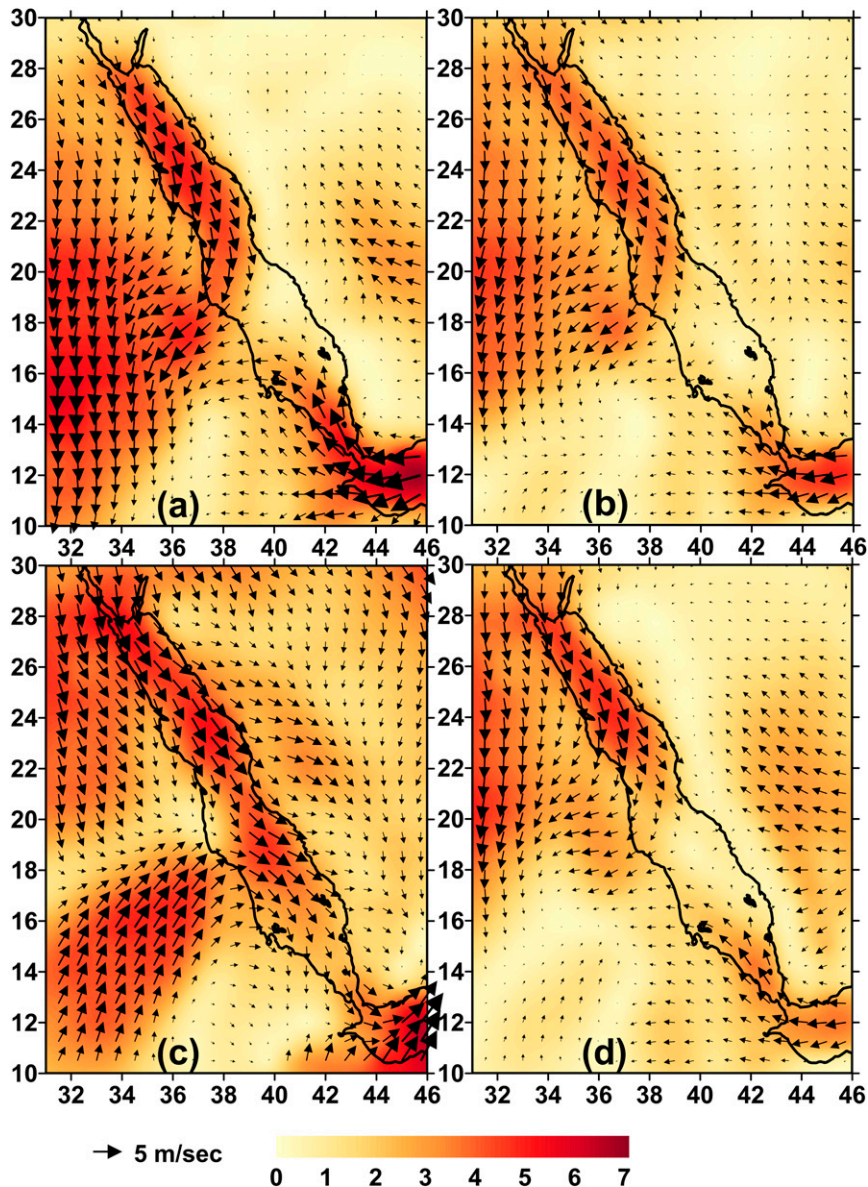


FIG. 3. ERA-Interim (1979–2013) wind climatology for (a) winter, (b) spring, (c) summer, and (d) autumn.

The MEI is based on both atmospheric and oceanic properties, the IMI only on atmospheric, and the IOD is a pure oceanic index. As the MEI, IOD, and IMI are not independent by definition, it is useful to investigate their level of mutual dependence and possible relationships with the other modes considered. Focusing only on the most influential indices (as derived in section 6b), Table 1 presents the correlation of NAO, EA, and EAWR with MEI, IOD, and IMI and the interrelation between MEI, IOD, and IMI based on monthly-mean index values for the period 1979–2013. The MEI, despite its potential wide-ranging ENSO-related impact, is independent of

both the NAO and EA and shows only a minor correlation with EAWR. The IOD has negligible correlation with the NAO, EA, and EAWR. Finally, the IMI shows a small but significant correlation with the NAO and EA and almost zero correlation with EAWR. Thus, the Indo-Pacific indices exhibit little or no relation with the NOAA/CPC modes of Northern Hemisphere atmospheric variability. On the other hand, the Indo-Pacific modes are expected to have a closer interrelation (e.g., Torrence and Webster 1999; Annamalai et al. 2003; Izumo et al. 2014). The values in Table 1 show that the MEI, IOD, and IMI correlate significantly with each

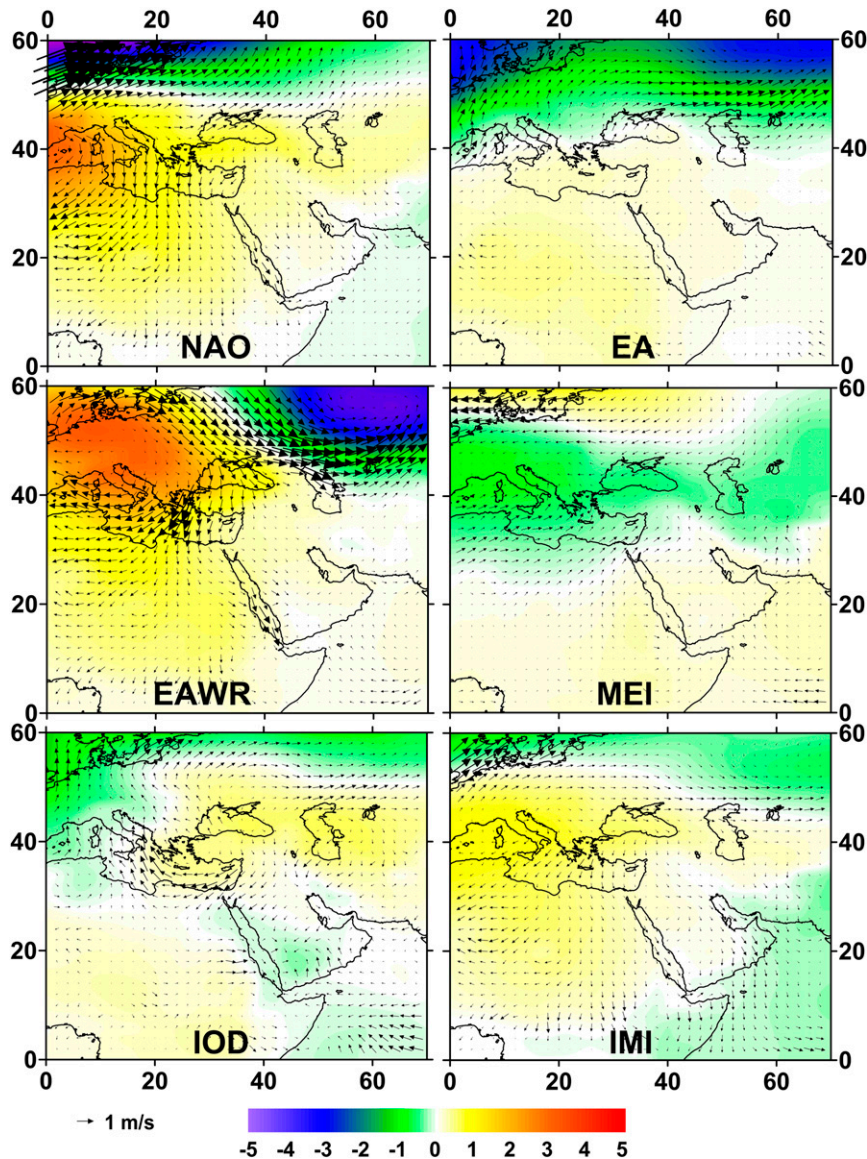


FIG. 4. SLP (color bar; hPa) and wind field anomalies for a unit positive index of the most influential indices during winter (DJF). SLP and wind are from ERA-Interim 1979–2013.

other, and the strongest correlation is found between MEI and IMI ($r = -0.43$).

6. Mode impacts on the Red Sea heat exchange

a. Basin and subbasin impacts

Before considering in detail the spatial distribution of climate mode impacts over the Red Sea, we quantify the basin- and subbasin-averaged values. These values reveal the general influence of the modes on the heat flux budget. Table 2 presents the net heat flux anomalies corresponding to a unit positive index averaged for the full Red

Sea basin and for the northern and southern subbasins. The anomalies are calculated for each season and for each dataset. The geographical latitude that separates the northern from the southern basin is defined to be 20°N. A total of nine climatic modes are considered (see section 2), but only six (NAO, EA, EAWR, MEI, IOD, and IMI) have a seasonal impact on the Red Sea surface heat exchange greater than 5 W m^{-2} (absolute value) for at least one subbasin. In winter, the NAO, EAWR, and IMI exhibit the most intense basinwide influence. All of them have their maximum impact on the northern part of the Red Sea, with the EAWR pattern being most influential with basin-averaged anomalies of -19 (-18) W m^{-2} per

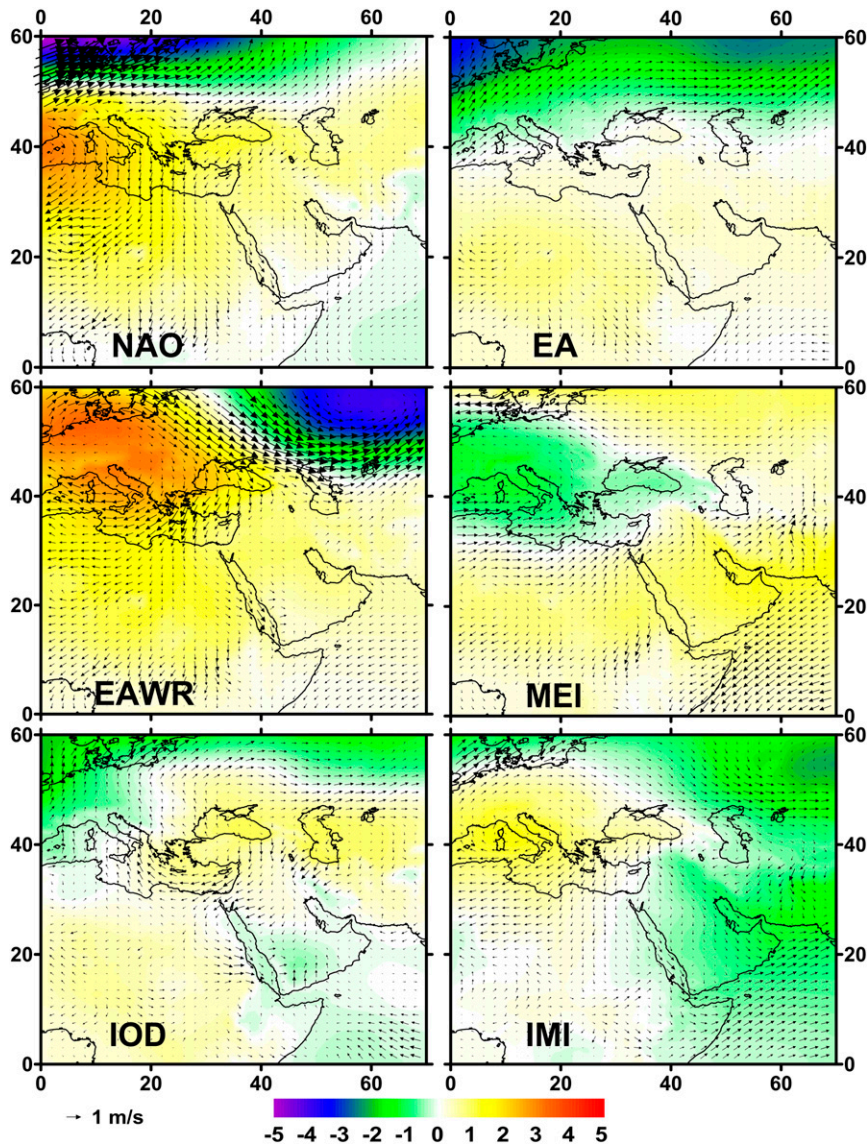


FIG. 5. SLP (color bar; hPa) and wind field anomalies for a unit positive index of the most influential indices during winter (DJF). SLP and wind are from MERRA 1979–2013.

index unit for MERRA (OAFflux). Spring, summer, and autumn are all characterized by lower impacts. In summer, the MEI has the strongest impact with values over the southern part of the Red Sea of 8 (13) W m^{-2} for MERRA (OAFflux).

b. Spatial distribution of the modes' impacts

To describe the seasonal and spatial variability of the modes' impacts, we show the net heat flux anomalies corresponding to a unit positive index during winter and summer for each grid point. Maps of the winter net heat flux anomaly based on the MERRA dataset are shown in Fig. 7. Statistically significant anomalies are calculated using a Student's t test at the confidence level of 95%. The

NAO and EAWR present a negative signal over the northern two-thirds (approximately north of 18°N) of the Red Sea in the sense that more positive NAO and EAWR values enhance the oceanic heat loss. However, the EAWR mode produces a stronger signal than the NAO and is also associated with positive anomalies over the southernmost part of the basin. The IMI pattern is very similar to the NAO pattern, as is to be expected given their significant correlation. All three modes (NAO, EAWR, and IMI) show local signals in the central-northern basin with anomaly maxima reaching -30 W m^{-2} for the EAWR. At the same time, and contrary to the EA, MEI, and IOD, they present statistical significance over most of the Red Sea. The behavior of

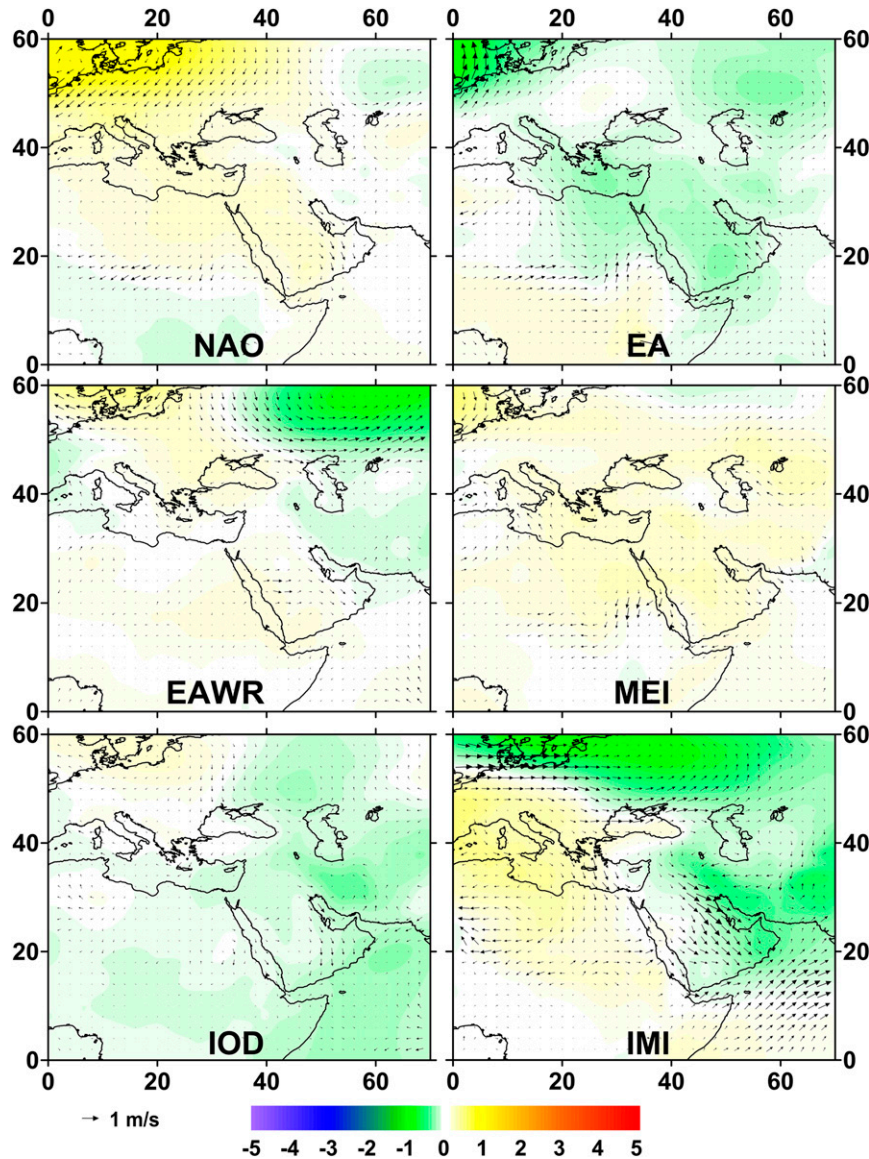


FIG. 6. As in Fig. 4, but during summer.

NAO and EAWR over the northern two-thirds of the Red Sea is in accordance with their behavior over the neighboring eastern Mediterranean Sea (JST11; Papadopoulos et al. 2012c). As regards the rest of the indices, the EA pattern has a minor basin-averaged impact, slightly positive over a small region at the northern edge of the basin, negative over the central part, and again positive in the south. Both MEI and IOD show a negative signal over the central part and positive in both the northern and southern parts. We have determined correlation coefficients between the mode index values and the basin-averaged winter-mean net heat flux. The EAWR has the strongest influence ($r = -0.63$, explaining 40% of the variance) followed by the NAO

($r = -0.41$, 17% of the variance); note that the negative correlation value arises because a positive value of the mode index corresponds to stronger heat loss, that is, a more negative net air–sea heat flux. Thus, the EAWR and NAO account for more than half (57%) of the variance in the Red Sea basin winter-mean net heat flux with smaller contributions (<5% per mode) from the other modes.

During summer, the spatially dependent impacts are typically weaker and show less significance than winter, consistent with the basin means. The EA and MEI are the most influential modes (Fig. 8). The NAO influence results in four successive domains of reverse sign extending along the longitudinal basin axis with signals

TABLE 1. Correlation coefficients between the modes employed in the study based on monthly-mean index values for the period 1979–2013. By definition NAO, EA, and EAWR have zero correlation between each other as orthogonal modes. Statistically significant ($p < 0.05$) coefficients are boldfaced.

Index	NAO	EA	EAWR	MEI	IOD
MEI	0.00	0.06	0.18	—	—
IOD	−0.06	0.07	0.09	0.24	—
IMI	0.23	0.13	0.04	−0.43	−0.21

locally exceeding 10 W m^{-2} (absolute values). The EA mode is associated with a positive signal over the northernmost edge and negative over the rest of the basin locally reaching -25 W m^{-2} . The MEI effects are similar to those induced by the NAO, but with a stronger positive signal that locally exceeds 20 W m^{-2} along the African coast in the southern part. The EAWR and IOD have a weak positive effect almost throughout the basin. Finally, the IMI impact is qualitatively similar, although weaker in magnitude than those induced by NAO and MEI. In comparison to the winter, the summer signals are considerably weaker, implying a more stable atmospheric circulation during this time of the year. Similar results are obtained for both seasons when the OAFflux dataset is employed (not shown).

c. Manifestation of the atmospheric forcing

For a more detailed understanding of how the atmospheric forcing affects the surface heat flux over the Red Sea, we investigate the relative contribution of each one of the net heat flux components. The net heat flux Q_{net} is the sum of four components:

$$Q_{\text{net}} = Q_s + Q_b + Q_e + Q_h,$$

where Q_s is the shortwave radiation, Q_b is the longwave radiation, Q_e is the latent heat (or evaporative heat), and Q_h is the sensible heat. The terms Q_s and Q_b are the radiative terms, and Q_e and Q_h are the turbulent terms. The radiative terms variability depends mostly on the fraction of cloud coverage and less on the specific humidity and air and sea surface temperature. On the other hand, the turbulent factors depend on the wind speed, specific humidity, and the temperature difference between air and sea surface. P13 point out that during winter over most of the Red Sea the turbulent components show much higher variability compared with their radiative counterparts. Thus, the turbulent components are expected to be the major factor driving the net heat flux anomalies. Analysis of the impact of the climatic modes on each one of the heat flux components shows that the latent heat determines the

TABLE 2. Seasonal basin- and subbasin-averaged net heat flux for a unit positive value of the employed indices; values greater than 5 W m^{-2} are boldfaced and greater in size.

		Index						
		NAO	EA	EAWR	MEI	IOD	IMI	
Winter	Full basin	MERRA	−9	−1	−13	1	−1	−9
		OAFflux	−10	−6	−12	−1	−4	−10
	North basin	MERRA	−13	−1	−19	1	−2	−13
		OAFflux	−14	−10	−18	−1	−8	−16
	South basin	MERRA	−6	−1	−7	1	1	−5
		OAFflux	−5	−3	−6	−2	0	−4
Spring	Full basin	MERRA	−2	0	−1	5	1	−5
		OAFflux	−1	−2	−2	3	1	−2
	North basin	MERRA	−3	1	−3	5	1	−5
		OAFflux	−1	−1	−3	4	0	−4
	South basin	MERRA	−1	−1	1	5	0	−4
		OAFflux	0	−3	−1	1	2	−1
Summer	Full basin	MERRA	1	−4	−1	4	−3	−1
		OAFflux	3	−4	2	10	−7	4
	North basin	MERRA	0	−1	−3	0	−3	0
		OAFflux	−1	−6	−1	7	−6	1
	South basin	MERRA	2	−8	0	8	−3	−2
		OAFflux	7	−1	5	13	−8	7
Autumn	Full basin	MERRA	−4	−3	2	1	−1	−4
		OAFflux	−3	−4	6	1	−5	−2
	North basin	MERRA	−9	−7	3	1	−2	−13
		OAFflux	−7	−8	7	1	−2	−11
	South basin	MERRA	2	1	1	2	1	5
		OAFflux	1	0	5	1	−7	8

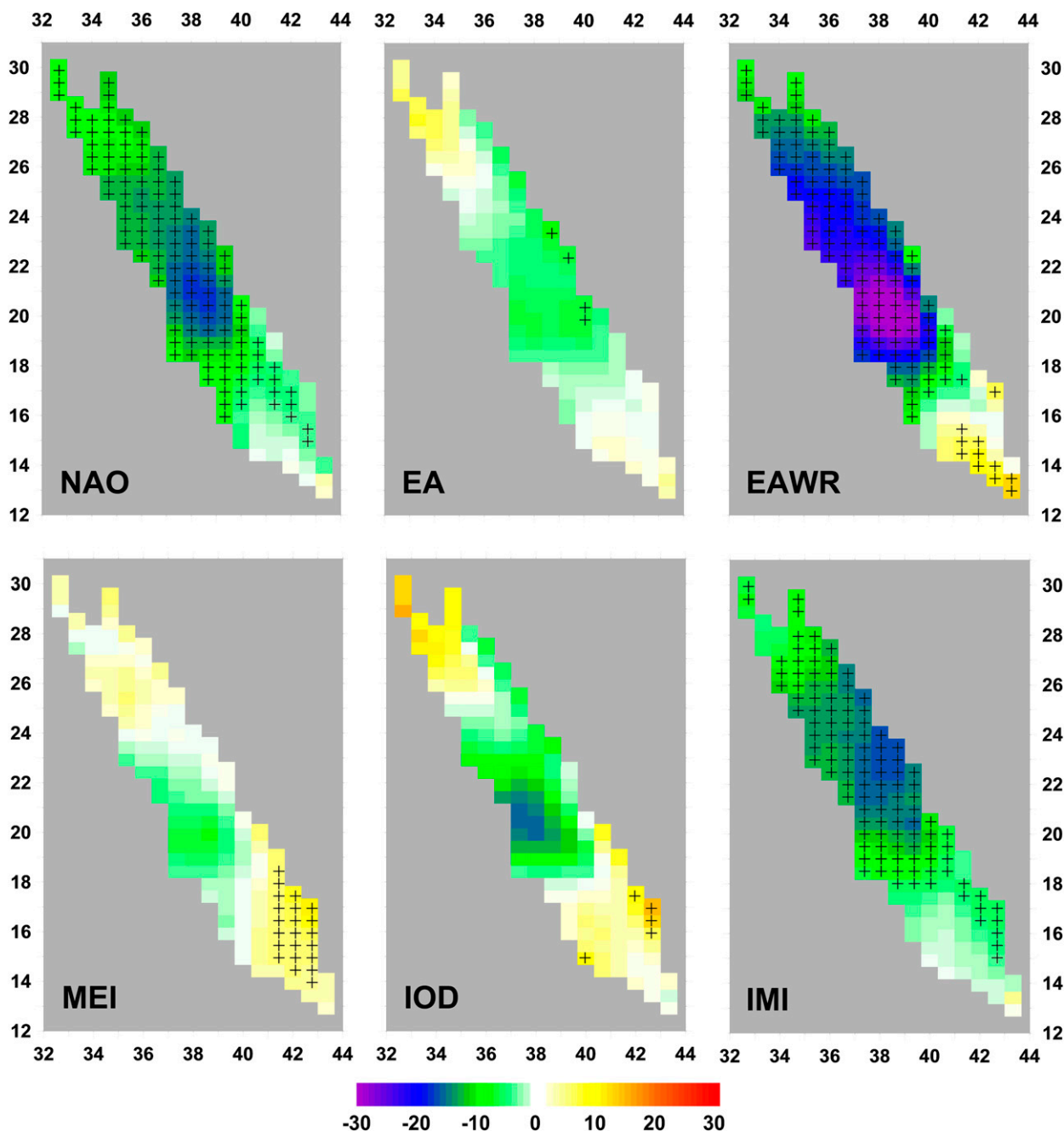


FIG. 7. MERRA winter (DJF) net heat flux ($W m^{-2}$) anomalies for a unit positive index. Anomalies marked with a plus sign are statistically significant at a confidence level of 95%.

mode-related normalized anomalies. This is more evident during winter and over the northern part of the basin and less evident during summer and over the southern part where the shortwave radiation presents a considerable contribution to the net flux anomalies. As a demonstration, we display the normalized anomalies separately for each component for the basinwide, most influential modes during winter and summer.

Figure 9 illustrates the winter unit impact of the most influential EAWR mode on each of the four components. It is clear that the net heat flux normalized anomalies (see EAWR panel in Fig. 7) are regulated by the latent heat (Fig. 9c). We show a similar picture for the MEI during summer (Fig. 10), in which the shortwave radiation has a significant contribution over the southern half of the basin.

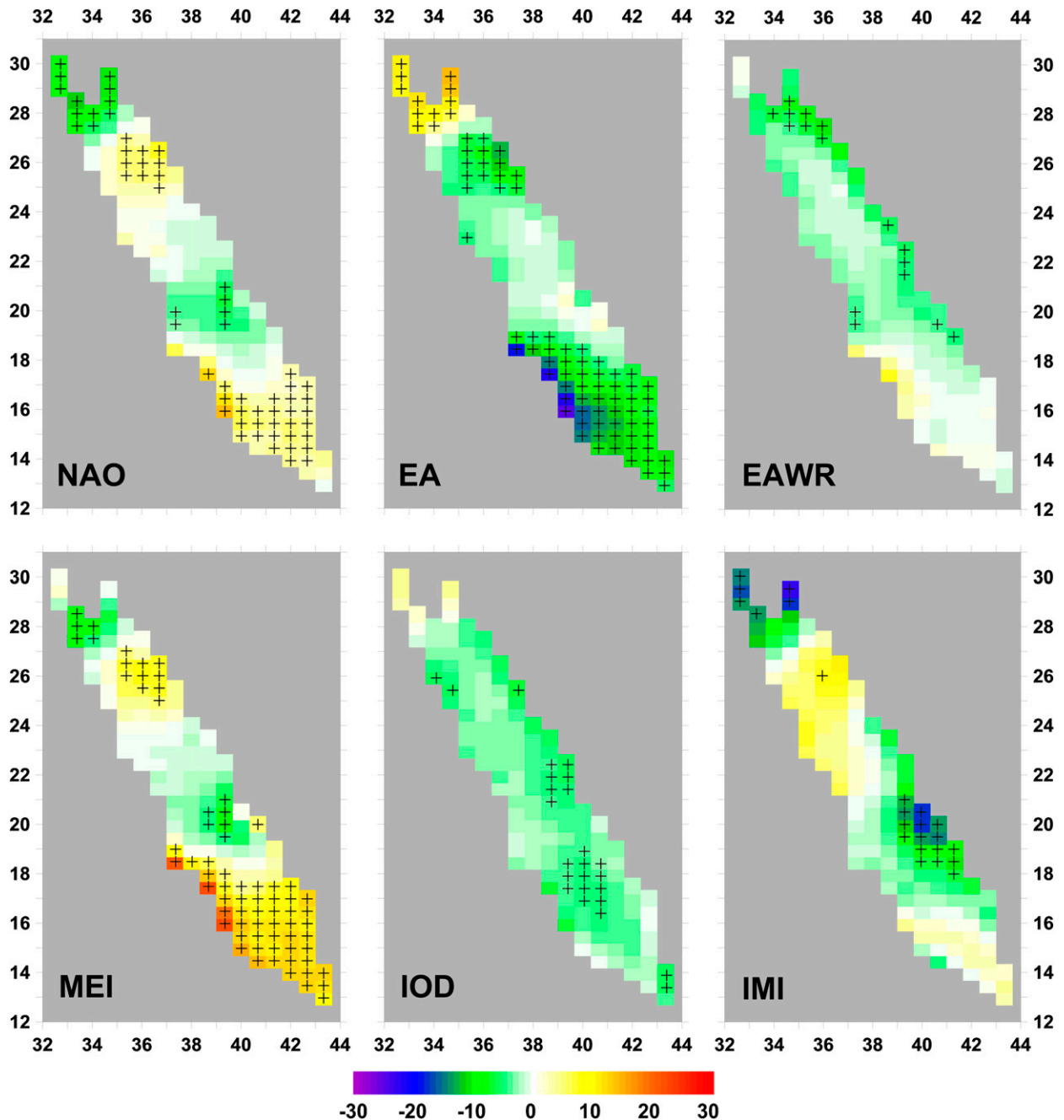


FIG. 8. As in Fig. 7, but for summer (JJA).

The dependence of the latent heat flux on the driving meteorological variables is given by the following equation (see, e.g., Josey et al. 2013):

$$Q_e = \rho_a c_e L U (q_a - q_s), \quad (1)$$

where ρ_a is the air density, c_e is a dimensionless coefficient (also known as the Dalton number), L is the latent heat constant, U is the wind speed at the height of 10 m, q_s is the

saturation-specific humidity calculated for the sea surface temperature, and q_a is the specific humidity of the overlying atmospheric air with $q_a \leq q_s$. To further investigate the role of the latent heat in determining the net heat flux anomalies over the Red Sea, we investigate the climate mode impacts on U and $q_a - q_s$. Figures 11 and 12 show the unit impact of the modes on these two terms for winter and summer. A comparison of Figs. 7 and 11 reveals that the normalized anomaly of the net heat flux follows the

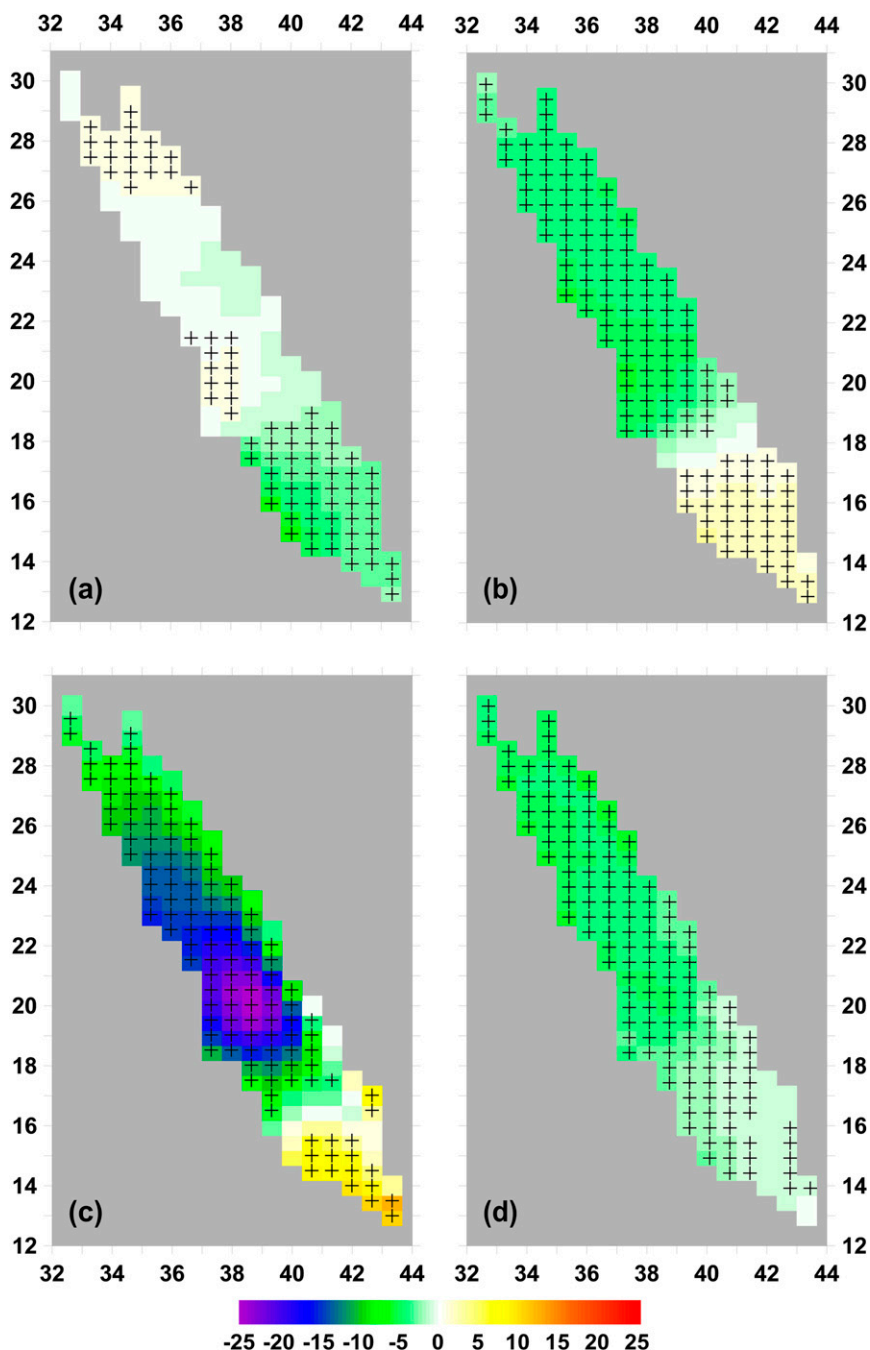


FIG. 9. MERRA winter (DJF) positive unit impact (W m^{-2}) of EAWR on (a) shortwave radiation, (b) longwave radiation, (c) latent heat, and (d) sensible heat. Impacts marked with a plus sign are statistically significant at a confidence level of 95%.

combined influence of the $q_a - q_s$ and wind fields. This comparison also demonstrates the prominent role of NAO, EAWR, and IMI during winter and MEI during summer. It is also apparent that the wind flow direction has a strong influence on the specific humidity. An example is the wind anomaly caused by the EA pattern over the central Red Sea during summer. In that case, an eastward wind anomaly

transfers dry air masses from Africa to the Red Sea, lowering the specific humidity along the African coast.

7. Concluding remarks

The influence on air–sea heat fluxes over the Red Sea of a range of climatic modes has been examined. The

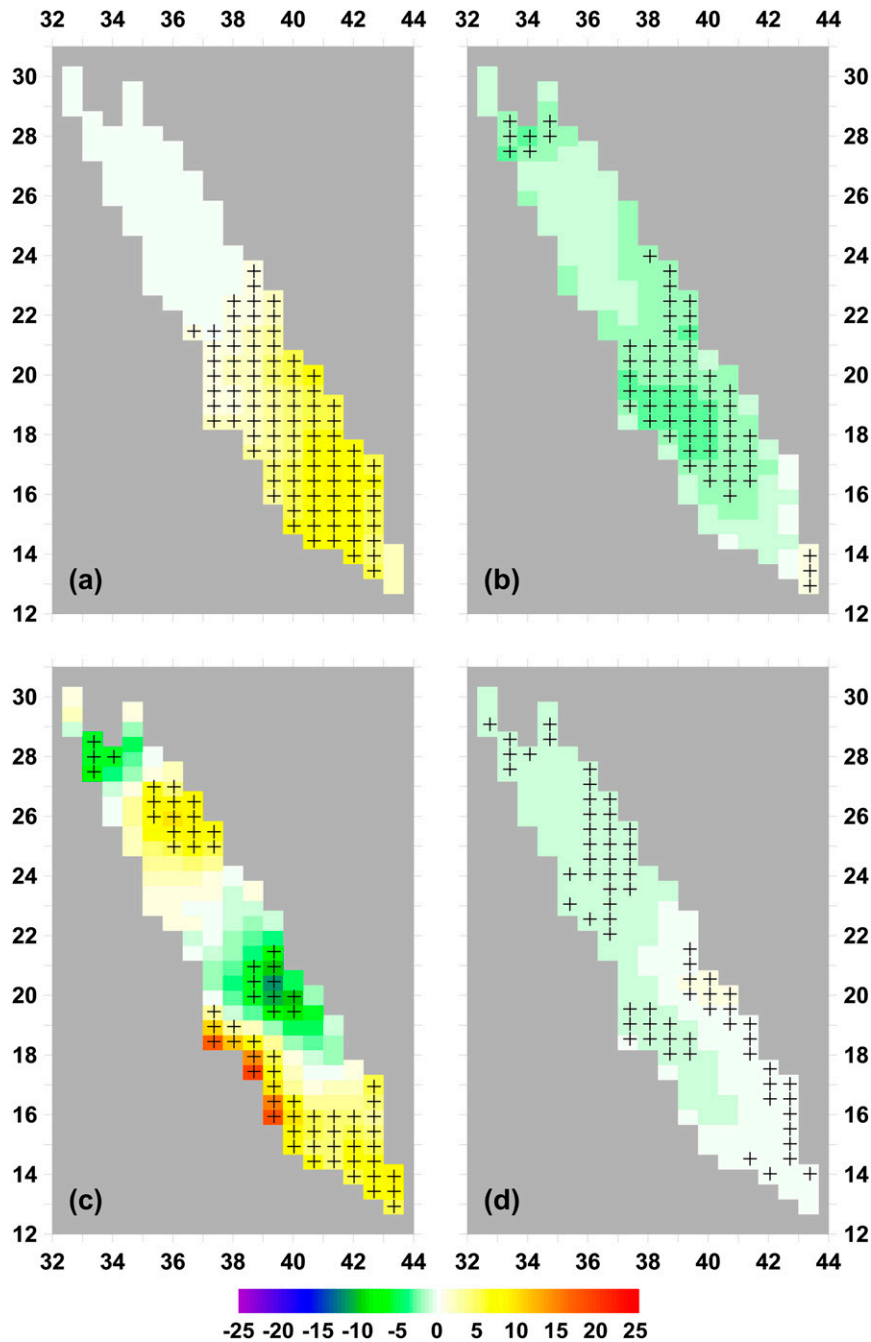


FIG. 10. As in Fig. 9, but for MEI during summer (JJA).

method employed by JST11 in the Mediterranean Sea that considers the impact on the air–sea heat flux corresponding to a positive unit of the index was followed. The potential impacts of a total of nine climatic modes were investigated on a typical seasonal basis. The vicinity of the Red Sea with the Indian Ocean dictates the employment of more climatic indices of Indo-Pacific origin. The mode impacts are strongest during winter,

when the NAO, EAWR, and IMI are all associated with heat flux anomalies ranging from -12 to -18 W m^{-2} per index unit over the northern basin. Smaller signals are observed during the spring when none of the indices show a basin- or subbasin-averaged value greater in magnitude than 5 W m^{-2} . Summer impacts are also lower than winter, and the MEI is the most influential index, particularly over the southern half of the basin.

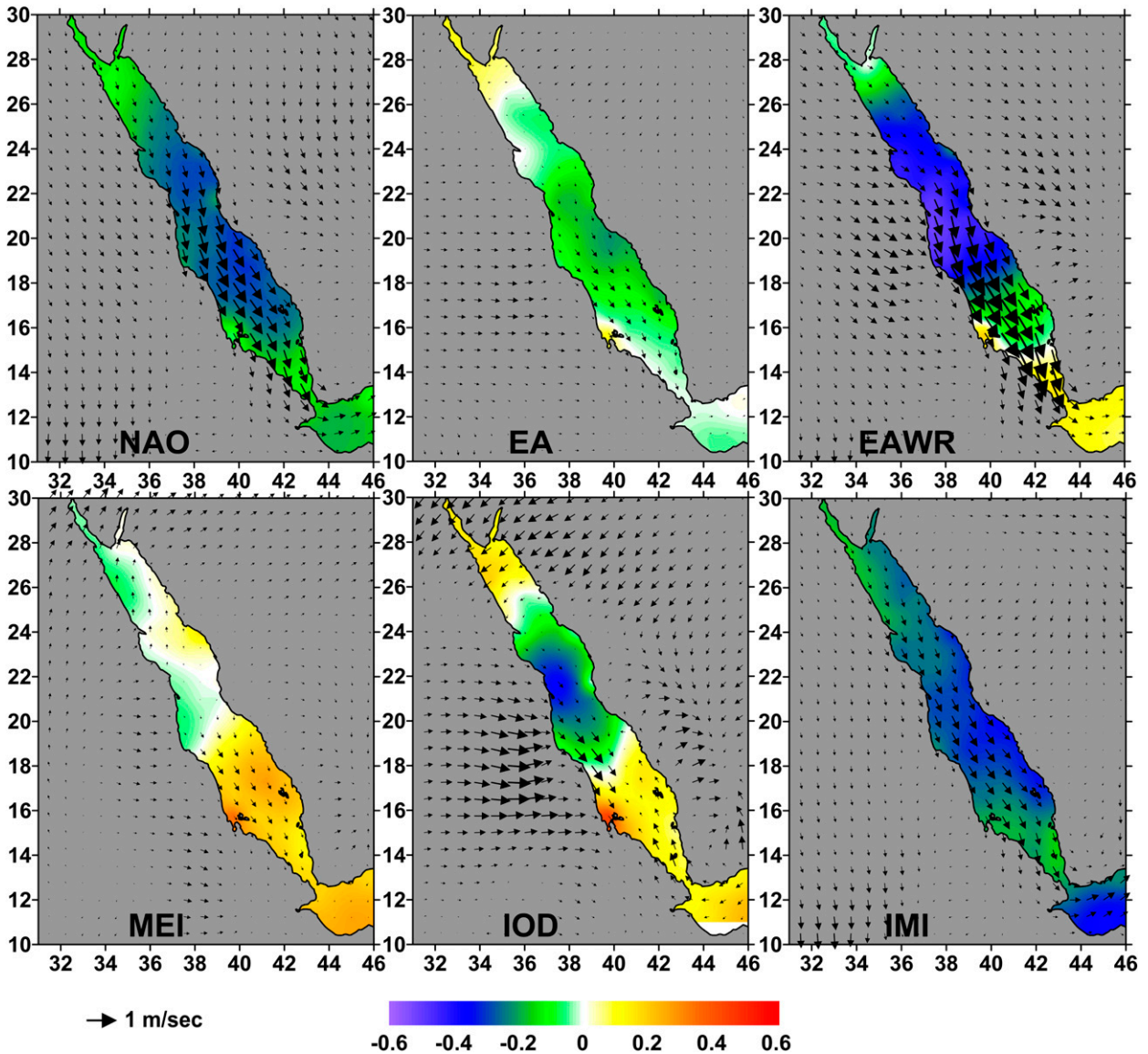


FIG. 11. Impact of the positive unit index on the $q_a - q_s$ (g kg^{-1}) and on the wind field during winter (DJF). The q_a , q_s , and wind are from ERA-Interim 1979–2013.

Winter impacts are also found to be stronger than summer in the Mediterranean Sea (JST11). In terms of the full basin effects, the NAO, EAWR, and IMI have the leading winter impacts of -10 , -12 , and -9 W m^{-2} per index unit, respectively. The mode impacts are primarily due to the latent heat flux component of the net heat exchange that in turn is driven by the influence of the specific humidity and wind fields.

The negative heat flux anomalies generated by the NAO and EAWR indicate that these modes are associated with a greater heat loss by the sea during winter. This is because of the transfer of colder air masses from higher latitudes during the positive phase of the NAO

and EAWR over a broader region including the eastern Mediterranean Sea (JST11; Papadopoulos et al. 2012c; Kontoyiannis et al. 2012). The SLP anomaly patterns associated with the positive phases of the two indices indicate that a transfer of cold air is favored, especially over the northern Red Sea, thanks to SLP increasing over areas north and west of the Red Sea. In addition, the IMI that correlates positively with both NAO and EA reinforces this effect. The most prominent difference between the two basins is the EA behavior, which has a major impact on the Mediterranean Sea but very weak impact on the Red Sea. To conclude, we restate our main result that is that analysis of both the MERRA and

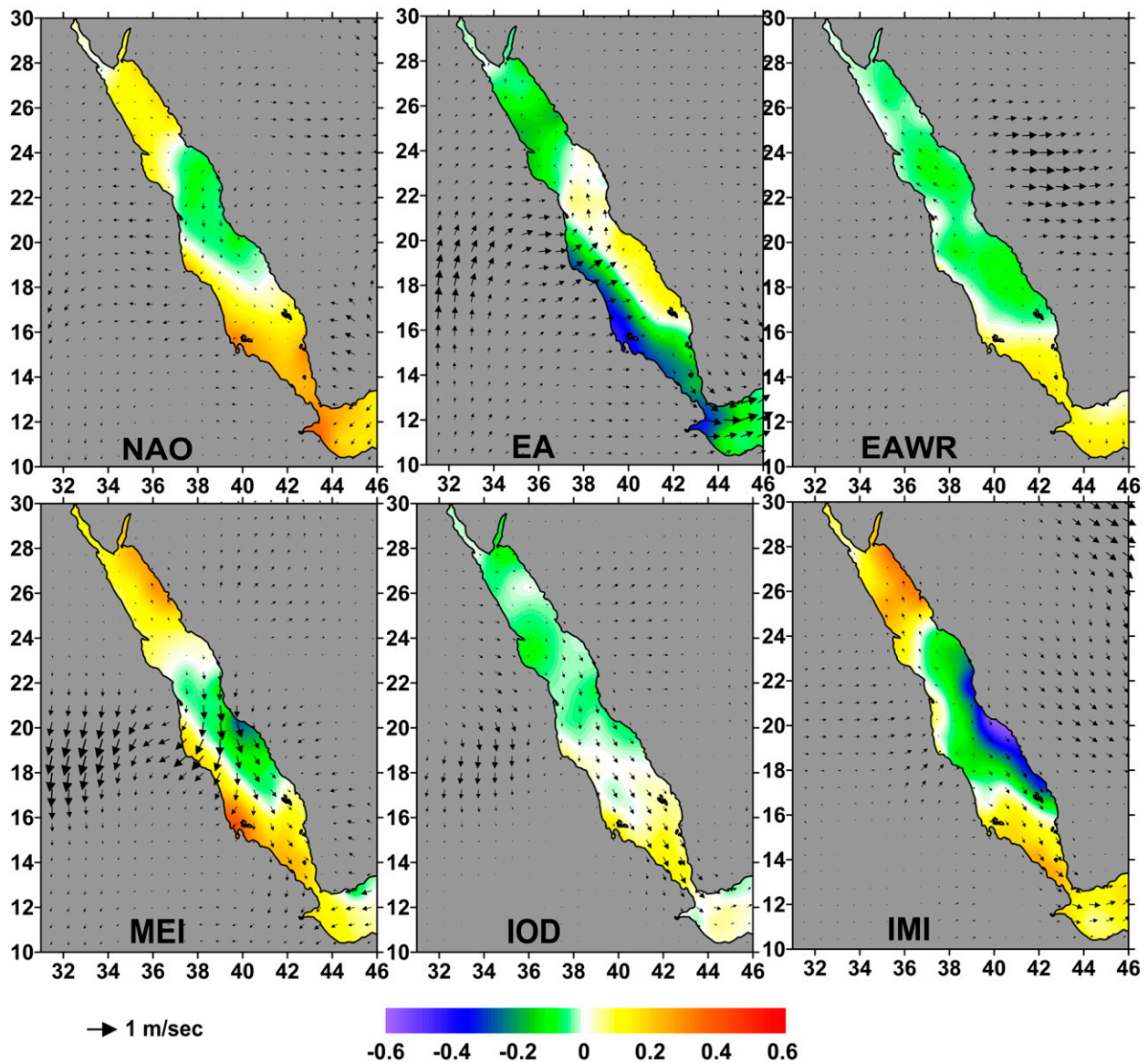


FIG. 12. As in Fig. 11, but for the summer (JJA).

OAFlux datasets has revealed a consistent picture in which the Red Sea surface heat exchange is mainly influenced by the NAO, EAWR, and IMI climatic modes during winter and the MEI during summer.

Acknowledgments. The authors thank the three anonymous reviewers for their valued contribution to the improvement of the manuscript.

REFERENCES

- Ahmad, F., and S. A. R. Sultan, 1989: Surface heat fluxes and their comparison with the oceanic heat flow in the Red Sea. *Oceanol. Acta*, **12** (1), 33–36.
- Alexander, M. A., and J. D. Scott, 1997: Surface flux variability over the North Pacific and North Atlantic Oceans. *J. Climate*, **10**, 2963–2978, doi:10.1175/1520-0442(1997)010<2963:SFVOTN>2.0.CO;2.
- Annamalai, H., R. Murtugudde, J. Potemra, S. P. Xie, P. Liu, and B. Wang, 2003: Coupled dynamics in the Indian Ocean: Spring initiation of the zonal mode. *Deep-Sea Res.*, **50**, 2305–2330, doi:10.1016/S0967-0645(03)00058-4.
- Barnston, A. G., and R. E. Livezey, 1987: Classification, seasonality and persistence of low-frequency atmospheric circulation patterns. *Mon. Wea. Rev.*, **115**, 1083–1126, doi:10.1175/1520-0493(1987)115<1083:CSAPOL>2.0.CO;2.
- Belkin, I. M., 2009: Rapid warming of large marine ecosystems. *Prog. Oceanogr.*, **81**, 207–213, doi:10.1016/j.pocean.2009.04.011.
- Bond, N. A., and M. F. Cronin, 2008: Regional weather patterns during anomalous air–sea fluxes at the Kuroshio Extension

- Observatory (KEO). *J. Climate*, **21**, 1680–1697, doi:10.1175/2007JCLI1797.1.
- Cayan, D. R., 1992: Latent and sensible heat flux anomalies over the northern oceans: The connection to monthly atmospheric circulation. *J. Climate*, **5**, 354–369, doi:10.1175/1520-0442(1992)005<0354:LASHFA>2.0.CO;2.
- Clifford, M., C. Horton, J. Schmitz, and L. H. Kantha, 1997: An oceanographic nowcast/forecast system for the Red Sea. *J. Geophys. Res.*, **102**, 25 101–25 122, doi:10.1029/97JC01919.
- Dee, D. P., and Coauthors, 2011: The ERA-Interim reanalysis: Configuration and performance of the data assimilation system. *Quart. J. Roy. Meteor. Soc.*, **137**, 553–597, doi:10.1002/qj.828.
- Izumo, T., M. Lengaigne, J. Vialard, J.-J. Luo, T. Yamagata, and G. Madec, 2014: Influence of Indian Ocean dipole and Pacific recharge on following year's El Niño: Interdecadal robustness. *Climate Dyn.*, **42**, 291–310, doi:10.1007/s00382-012-1628-1.
- Josey, S. A., 2003: Changes in the heat and freshwater forcing of the eastern Mediterranean and their influence on deep water formation. *J. Geophys. Res.*, **108**, 3237–3259, doi:10.1029/2003JC001778.
- , and R. Marsh, 2005: Surface freshwater flux variability and recent freshening of the North Atlantic in the eastern subpolar gyre. *J. Geophys. Res.*, **110**, C05008, doi:10.1029/2004JC002521.
- , S. Somot, and M. Tsimplis, 2011: Impacts of atmospheric modes of variability on Mediterranean Sea surface heat exchange. *J. Geophys. Res.*, **116**, C02032, doi:10.1029/2010JC006685.
- , S. Gulev, and L. Yu, 2013: Exchanges through the ocean surface. *Ocean Circulation and Climate: A 21st Century Perspective*, 2nd ed. G. Siedler et al., Eds., Academic Press, 115–140.
- Kontoyiannis, H., V. Papadopoulos, A. Kazmin, A. Zatsepin, and D. Georgopoulos, 2012: Climatic variability of the sub-surface sea temperatures in the Aegean-Black Sea system and relation to meteorological forcing. *Climate Dyn.*, **39**, 1507–1525, doi:10.1007/s00382-012-1370-8.
- Lim, Y.-K., 2014: The east Atlantic/west Russia (EA/WR) teleconnection in the North Atlantic: Climate impact and relation to Rossby wave propagation. *Climate Dyn.*, doi:10.1007/s00382-014-2381-4.
- Martínez-Asensio, A., M. Marcos, M. N. Tsimplis, D. Gomis, S. A. Josey, and G. Jordà, 2014: Impact of the atmospheric climate modes on Mediterranean sea level variability. *Global Planet. Change*, **118**, 1–15, doi:10.1016/j.gloplacha.2014.03.007.
- Morcos, S. A., 1970: Physical and chemical oceanography of the Red Sea. *Oceanogr. Mar. Biol. Annu. Rev.*, **8**, 73–202.
- Murray, S. P., and W. Johns, 1997: Direct observations of seasonal exchange through the Bab el Mandeb strait. *Geophys. Res. Lett.*, **24**, 2557–2560, doi:10.1029/97GL02741.
- Papadopoulos, V. P., A. Bartzokas, T. Chronis, D. Georgopoulos, and G. Ferentinos, 2012a: Factors regulating the air–sea heat fluxes in the Aegean Sea. *J. Climate*, **25**, 491–508, doi:10.1175/2011JCLI4197.1.
- , S. A. Josey, A. Bartzokas, S. Somot, S. Ruiz, and P. Drakopoulou, 2012b: Large-scale atmospheric circulation favoring deep and intermediate water formation in the Mediterranean Sea. *J. Climate*, **25**, 6079–6091, doi:10.1175/JCLI-D-11-00657.1.
- , H. Kontoyiannis, S. Ruiz, and N. Zarokanellos, 2012c: Influence of atmospheric circulation on turbulent air-sea heat fluxes over the Mediterranean Sea during winter. *J. Geophys. Res.*, **117**, C03044, doi:10.1029/2011JC007455.
- , Y. Abualnaja, S. A. Josey, A. Bower, D. E. Raitsos, H. Kontoyiannis, and I. Hoteit, 2013: Atmospheric forcing of the winter air–sea heat fluxes over the northern Red Sea. *J. Climate*, **26**, 1685–1701, doi:10.1175/JCLI-D-12-00267.1.
- Patzert, W. C., 1974: Wind-induced reversal in Red Sea circulation. *Deep-Sea Res. Oceanogr. Abstr.*, **21**, 109–121, doi:10.1016/0011-7471(74)90068-0.
- Raitsos, D. E., I. Hoteit, P. K. Prihartato, T. Chronis, G. Triantafyllou, and Y. Abualnaja, 2011: Abrupt warming of the Red Sea. *Geophys. Res. Lett.*, **38**, L14601, doi:10.1029/2011GL047984.
- Rienecker, and Coauthors, 2011: MERRA: NASA's Modern-Era Retrospective Analysis for Research and Applications. *J. Climate*, **24**, 3624–3648, doi:10.1175/JCLI-D-11-00015.1.
- Rogers, J. C., 1990: Patterns of low-frequency monthly sea level pressure variability (1899–1986) and associated wave cyclone frequencies. *J. Climate*, **3**, 1364–1379, doi:10.1175/1520-0442(1990)003<1364:POLFMS>2.0.CO;2.
- Saji, N. H., B. N. Goswami, P. N. Vinayachandran, and T. Yamagata, 1999: A dipole mode in the tropical Indian Ocean. *Nature*, **401**, 360–363.
- Sofianos, S. S., and W. E. Johns, 2002: An oceanic general circulation model (OGCM) investigation of the Red Sea circulation, 1. Exchange between the Red Sea and the Indian Ocean. *J. Geophys. Res.*, **107**, 3196, doi:10.1029/2001JC001184.
- , and —, 2003: An oceanic general circulation model (OGCM) investigation of the Red Sea circulation: 2. Three dimensional circulation in the Red Sea. *J. Geophys. Res.*, **108**, 3066, doi:10.1029/2001JC001185.
- Torrence, C., and P. J. Webster, 1999: Interdecadal changes in the ENSO–monsoon system. *J. Climate*, **12**, 2679–2690, doi:10.1175/1520-0442(1999)012<2679:ICITEM>2.0.CO;2.
- Wang, B., and Z. Fan, 1999: Choice of South Asian summer monsoon indices. *Bull. Amer. Meteor. Soc.*, **80**, 629–638, doi:10.1175/1520-0477(1999)080<0629:COSASM>2.0.CO;2.
- Wolter, K., and M. S. Timlin, 2011: El Niño/Southern Oscillation behaviour since 1871 as diagnosed in an extended multivariate ENSO index (MEI.ext). *Int. J. Climatol.*, **31**, 1074–1087, doi:10.1002/joc.2336.
- Yao, F., I. Hoteit, L. J. Pratt, A. S. Bower, P. Zhai, A. Köhl, and G. Gopalakrishnan, 2014a: Seasonal overturning circulation in the Red Sea: 1. Model validation and summer circulation. *J. Geophys. Res. Oceans*, **119**, 2238–2262, doi:10.1002/2013JC009004.
- , —, —, —, A. Köhl, G. Gopalakrishnan, and D. Rivas, 2014b: Seasonal overturning circulation in the Red Sea: 2. Winter circulation. *J. Geophys. Res. Oceans*, **119**, 2263–2289, doi:10.1002/2013JC009331.
- Yu, L., X. Jin, and R. A. Weller, 2008: Multidecade global flux datasets from the Objectively Analyzed Air–Sea Fluxes (OAFlux) project: Latent and sensible heat fluxes, ocean evaporation, and related surface meteorological variables. Woods Hole Oceanographic Institution OAFlux Project Tech. Rep. OA-2008-01, 64 pp.
- Zhang, Y.-C., W. B. Rossow, A. A. Lacis, V. Oinas, and M. I. Mishchenko, 2004: Calculation of radiative fluxes from the surface to top of atmosphere based on ISCCP and other global data sets: Refinements of the radiative transfer model and the input data. *J. Geophys. Res.*, **109**, D19105, doi:10.1029/2003JD004457.